2. Optical propagation through fog

As light propagates through the atmosphere, it can get scattered multiple times, which results in a glow around the light source in the image, as shown in Fig. 1. Multiple scattering can be neglected in clear air or light rain, but becomes particularly important in haze or fog. There are different approaches for modeling propagation of light with multiple scattering. One class of methods involves numerical Monte-Carlo ray-tracing simulation [17]. A drawback of such methods is their high computational complexity, which can grow exponentially with the number of scattering events to which a ray is subjected.
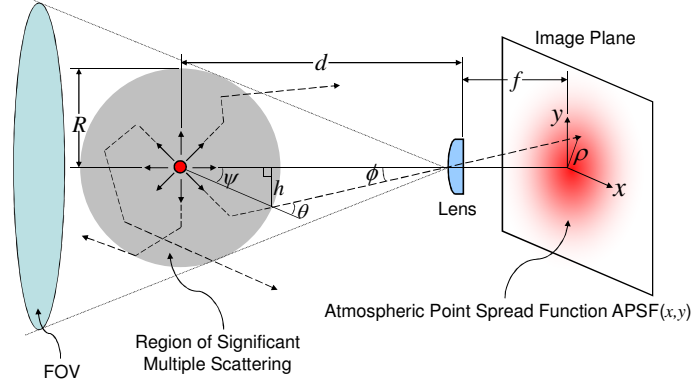

Fig. 1. As a result of the multiple scattering of light in the atmosphere, the image of a point source spreads out into a spot known as the atmospheric point spread function. When the distance between the transmitter and receiver is much larger than the focal length of the receiver lens, we can assume that multiple scattering only happens within a sphere around the source that fits into the FOV of the receiver (region of significant multiple scattering), and that the effect of propagation through the rest of the atmosphere is merely attenuation.

An alternate approach, which we pursue here, is based on solving the *radiative transfer equation* (RTE) [18]. When a ray of light enters a scattering particle, it can get scattered in multiple directions, as shown in Fig. 2. The intensity of light scattered in different directions depends on the *phase function* of the particle, which is defined as [18]

$$P(\cos\alpha) = P(\theta,\phi;\theta',\phi') = \frac{I(\theta,\phi)}{I(\theta',\phi')}, \tag{1}$$

where $I(\theta',\phi')$ is the intensity of the light incident along the direction (θ',ϕ') and $I(\theta,\phi)$ is the intensity of the light scattered along the direction (θ,ϕ). Under most atmospheric conditions, the phase function is only a function of α, which is the angle between the incident and scattered rays. It can be shown that the cosine of this angle can be expressed in terms of the directions of the incident and scattered light, as

$$\cos\alpha = \mu\mu' + \sqrt{(1-\mu^2)(1-\mu'^2)}\cos(\phi-\phi'), \tag{2}$$
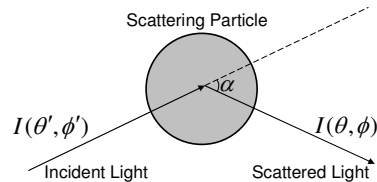
where $\mu = \cos\theta$ and $\mu' = \cos\theta'$.

Fig. 2. The phase function $P(\cos\alpha)$ is the ratio of the intensity of light scattered at an angle α to the intensity of the incident light.

The change in the radiance of light propagating in each direction at each point in space is governed by the RTE. The general form of the RTE is [18]

$$-\frac{dI}{\sigma\,ds} = I - F,$$

(3)

where I is the radiance (W/m²·sr), ds is a differential length element in the direction (θ, ϕ) and σ is an *extinction coefficient*, which is related to the *visibility range* of the atmosphere, V, by

$$\sigma = \frac{3.912}{V} \qquad (\text{m}^{-1}).$$

(4)

Also, $F(\theta, \phi)$ is the *source function* defined by

$$F(\theta, \phi) = \frac{1}{4\pi} \int_0^{2\pi} \int_0^\pi P(\cos\alpha) I(\theta', \phi')\, d\theta' d\phi'.$$

(5)

When a light source is isotropic and the medium in which the light propagates has spherical symmetry, the radiance at each point in space is only a function of the distance from the source, R, and the angle with respect to the radial direction, θ. In this case, ds describes an element of length in the direction θ at a distance R from the source, and we have

$$dR = \cos\theta\,ds \qquad \text{and} \qquad R\,d\theta = -\sin\theta\,ds.$$

(6)

Therefore, the RTE becomes

$$\cos\theta\frac{\partial I}{\partial R} - \frac{\sin\theta}{R}\frac{\partial I}{\partial \theta} = -\sigma\big[I(R,\theta) - F(R,\theta)\big].$$

(7)

Writing the RTE in terms of μ, as defined above, and defining an *optical thickness* $T = \sigma R$, we obtain

$$\mu\frac{\partial I}{\partial T} + \frac{1-\mu^2}{T}\frac{\partial I}{\partial \mu} = -I(T,\mu) + \frac{1}{4\pi}\int_0^{2\pi}\int_{-1}^1 P(\cos\alpha) I(T,\mu')\, d\mu' d\theta'.$$

(8)

Different phase functions are used to describe scattering in different media. It has been shown that the Henyey-Greenstein phase function can model very well a wide range of atmospheres, from clear air to dense fog [19]. This phase function is given by

$$P(\cos\alpha) = \frac{1-q^2}{\left(1 + q^2 - 2q\cos\alpha\right)^{3/2}}.$$

(9)

Here, q is a *forward scattering parameter*, lying between 0 and 1, which determines how much light scatters in different directions as it propagates. For $q = 0$, light is scattered isotropically in all directions, whereas for $q = 1$, all the light is scattered in the forward direction. Different values of q model different types of atmospheres, and the value of q is closely related to the size and texture of the scattering particles [20]. For example, a value of q between 0.1 and 0.6 can model a misty or hazy atmosphere, while a value between 0.7 and 0.9 models light to heavy fog [21]. The optical thickness T determines how much light is attenuated during propagation, and is more related to the density of the scattering particles [20]. In the RTE formulation, the optical thickness T and the forward scattering parameter q completely determine propagation of light in the atmosphere.

Narasimhan and Nayar [22] have shown that for an isotropic point source, by expanding the Henyey-Greenstein phase function in a series of Legendre polynomials, the following solution to the RTE is obtained:

$$I(T,\mu) = I_0 \sum_{n=0}^{\infty} \left(g_n(T) + g_{n+1}(T)\right)L_n(\mu),$$ (10)

where I_0 is the radiant intensity of the isotropic source (W/sr), $L_n(\cdot)$ is the Legendre polynomial of order n, and

$$g_0(T) = 0$$
$$g_n(T) = \exp\left(-\beta_n T - \alpha_n \ln T\right), n \neq 0$$
$$\alpha_n = n + 1$$
$$\beta_n = \frac{2n+1}{n}\left(1 - q^{n-1}\right).$$ (11)

Closed-form approximations have been used to speed up computation of (10) in some applications, such as computer vision [23].

The image of a point source with unit radiant intensity obtained in an imaging system under a given atmospheric condition is called the *atmospheric point spread function* (APSF). The importance of the APSF is that if it is known for a given atmospheric condition, then the image of any light source of arbitrary shape and size can be computed by a two-dimensional convolution. Given an imaging system, to find the APSF as a function of image-plane coordinates (x, y), on should project $I(T, \mu)$ onto the image plane, i.e., find a mapping between the variables (T, μ) and (x, y). It has been shown [22] that when the distance between the light source and the receiver, d, is much greater than the focal length of the lens in the receiver, f, one can assume that multiple scattering happens only inside a sphere that surrounds the source and lies within the receiver FOV. In Fig. 1, this sphere is indicated as the region of significant multiple scattering. The effect of propagation through the rest of the atmosphere can be modeled simply as a loss of $\exp(-T')$, where $T' = \sigma d$ is the optical thickness between the point source and imaging system. As seen in Fig. 1, assuming the point source is isotropic, because of azimuthal symmetry in the system, the APSF is only a function of the radial distance from the center of the image plane, $\rho = (x^2 + y^2)^{1/2}$. Working out the relationship between ρ and θ and considering multiple scattering only in the region of significant multiple scattering, we obtain

$$\text{APSF}(x, y) = \text{APSF}(\rho) = \frac{I(T, \mu(\rho))}{I_0}e^{-T'} \quad (\text{m}^{-2}),$$ (12)

where

$$\mu(\rho) = \cos\left(\theta(\rho)\right)$$
$$\theta(\rho) = \phi + \psi = \tan^{-1}\left(\frac{\rho}{f}\right) + \sin^{-1}\left(\frac{h}{R}\right)$$
$$h = \frac{b - \sqrt{b^2 - ac}}{a}$$
$$a = \rho^2 + f^2$$
$$b = d f \rho$$
$$c = \left(d^2 - R^2\right)\rho^2$$
$$R = d \sin\left(\frac{\text{FOV}}{2}\right).$$ (13)

Note that we have not explicitly shown the dependence of the APSF on q and T in the above equations. If we substitute the expression for $I(T,\mu)$ given by (10) into (12), we obtain the APSF for an arbitrary atmospheric condition and an arbitrary imaging system as a function of the coordinates on the image plane. Note also that the APSF, as defined here takes into account loss due to absorption in the atmosphere, but not the free-space path loss, which is proportional to $1/d^2$. We will consider the path loss separately in the expression for received optical power when analyzing an FSO link in the next section. Note also that the exact APSF of a system depends on source radiation pattern, and the APSF in (10) was derived for an isotropic source. When we analyze FSO links in the next section, however, we assume that the APSF derived here is also valid for a first-order Lambertian source. This assumption is justified by the observation that when the misalignment between transmitter and receiver is small, a Lambertian source would behave nearly identically to an isotropic source. The condition for the approximate validity of this APSF is defined in the next section.

Fig. 3 shows the cross section of the APSF for an imaging system using a 28-mm f/2.8 lens and an image sensor of size $19 \times 19\,\text{mm}^2$ in a thin $(T < 2)$ and a thick $(T > 3)$ atmosphere. It is seen that in a thin atmosphere, the full-width at half-maximum (FWHM) of the APSF depends strongly on q. As it is seen in Fig. 3(a), for an atmosphere with $T = 1.2$, the FWHM of the APSF is 3.9 mm, 3.4 mm and 2.4 mm for q equal to 0.2, 0.75 and 0.9, respectively. The FWHM of APSF is a measure of how much the image blooms due to the atmospheric condition. As expected, the FWHM is smaller for bigger values of the forward scattering parameter q, because particles with larger q tend to scatter light more in the forward direction and less in transverse directions.

In contrast to the thin-atmosphere regime, in the thick atmosphere regime, the FWHM of the APSF is nearly independent of the forward scattering parameter. As seen in Fig. 3(b), for a thick atmosphere with $T = 4.1$, the FWHM of the APSF is 7.3 mm for q equal to 0.2, 0.75 and 0.9. Comparison of the peak values of the APSF in Fig. 3(a) and 3(b) shows that the amount of attenuation strongly depends on the optical thickness, but depends only weakly on the forward scattering parameter. Note that the peak values of the APSF for $T = 4.1$ are about three orders of magnitude smaller than those for $T = 1.2$.

Thus far, we have discussed the effect of atmospheric effects on radiative transfer and showed how the RTE can be solved to find the APSF under certain assumptions. In the next section, we will discuss the impact of atmospheric effects on the performance of FSO links.
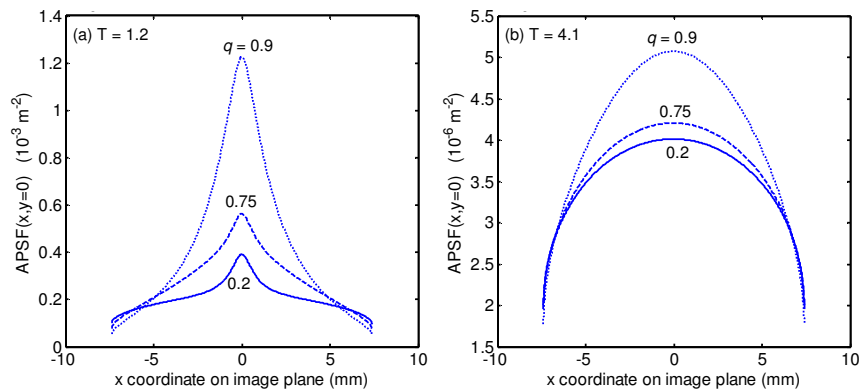

Fig. 3. Cross section of the APSF for (a) a thin atmosphere (T = 1.2) and (b) a thick atmosphere (T = 4.1). In a thick atmosphere, where the density of scatterers is high, the FWHM of the ASPF is almost independent of the value of the forward scattering parameter q. By contrast, in a thin atmosphere, where the density of the scatterers is low, the FWHM of the APSF is larger for smaller values of q.

3. Effect of fog on free-space optical links

3.1 Link analysis

In this section, in order to predict the performance, including the SNR or bit-error ratio (BER) of an optical link as a function of various parameters, we introduce a detailed model for the link and its components, including the transmitter and imaging receiver. The model presented here was first developed in [16].

Fig. 4 shows the general geometry of an FSO link. Assuming the line joining the transmitter to the receiver makes angles ϕ and ψ with respect to the transmitter and receiver surface normals, respectively, the total average power detected by the receiver (either imaging or non-imaging) is given by [16]

$$P_{\text{rec}} = I(\phi, d) T_F(\psi) T_L(\psi) A \cos \psi, \tag{14}$$

where $I(\phi, d)$ is the irradiance incident on the receiver (W/m^2), $T_F(\psi)$ is the optical filter transmission factor (W/W), $T_L(\psi)$ is the lens transmission factor (W/W) and A is the receiver light collection area at normal incidence (m^2). The transmission factors $T_F(\psi)$ and $T_L(\psi)$ lie between 0 and 1. The lens transmission factor rapidly approaches zero as the incidence angle ψ approaches the receiver FOV.
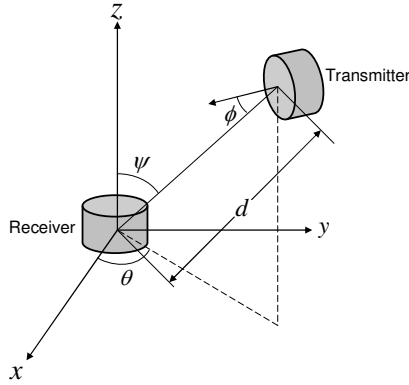

Fig. 4. Geometry of an FSO link.

If light enters the receiver through a lens having f-number N_f and focal length f, the light collection area is given by

$$A = \pi \left(\frac{f}{2N_f} \right)^2. \tag{15}$$

Assuming the transmitter uses LEDs, the irradiance at a distance R can be modeled by a generalized Lambertian pattern

$$I(\phi, d) = P_{\text{Tx}} \frac{(n+1)}{2\pi d^2} \cos^n \phi \qquad (\text{W/m}^2), \tag{16}$$

where P_{Tx} is the average transmitted optical power and n is related to the half-power semi-angle of the transmitter, $\Phi_{1/2}$, by $n = -\ln 2 / \ln(\cos \Phi_{1/2})$.

The image formed on the photodetector array in the absence of atmospheric effects is described by the irradiance distribution $I_{\text{rec}}(x, y)$. This image is a function of the geometry of the system, the lens focal length f, average received power P_{rec} and the atmospheric conditions. In the absence of fog, one can find an approximation to this image using well-known equations of geometrical optics. Throughout this work, we neglect lens aberrations,

whose effect is negligible in comparison to that of the atmospheric effects of interest. For example, assuming the transmitter emits light in a circular disk of uniform irradiance, the image is an ellipse of uniform irradiance, whose size and location can be found from the geometry of conic sections and the lens magnification. More generally, the image on the photodetector array can be expressed as

$$I_{\text{rec}}(x,y) = L(S, P_{\text{rec}}, f, d, \psi, \theta, \phi) \qquad (\text{W/m}^2), \tag{17}$$

where L is a linear operator that models the propagation of light from transmitter to the receiver based on geometrical optics, and S specifies the transmitter irradiance distribution (e.g., circular disk with uniform irradiance). Atmospheric effects, such as fog, can strongly affect the image formed on the photodetector array. Assuming atmospheric effects make the imaging process fully incoherent [18], by the principle of linear supersposition, the image formed in the presence of atmospheric effects is

$$I_{\text{rec,fog}}(x,y) = I_{\text{rec}}(x,y) * \text{APSF}(x,y), \tag{18}$$

where $*$ denotes a two-dimensional convolution and $\text{APSF}(x,y)$ is given by (12). The APSF (12), which was derived for an isotropic source, is assumed approximately valid for a first-order Lambertian source when the angle ϕ, as shown in Fig. 4, is small.

In an imaging receiver, the photodetector array has multiple pixels. The image of the transmitter, depending on its size and location, may overlap more than one pixel. The ith pixel receives a fraction of the total power that can be expressed as

$$P_{\text{rec},i} = \iint s_i(x,y) I_{\text{rec,fog}}(x,y) \, dxdy \qquad i = 1, 2, \cdots, N, \tag{19}$$

where the integral is carried over the photodetector, N is the number of pixels and $s_i(x,y)$ is an indicator function given by

$$s_i(x,y) = \begin{cases} 1, & \text{if } (x,y) \text{ in the interior of the } i^{\text{th}} \text{ pixel} \\ 0, & \text{otherwise} \end{cases} \tag{20}$$

The total noise variance in each pixel is given by,

$$\sigma_{\text{tot},i}^2 = \sigma_{\text{shot},i}^2 + \sigma_{\text{th},i}^2 \qquad i = 1, 2, \cdots, N, \tag{21}$$

where $\sigma_{\text{shot},i}^2$ and $\sigma_{\text{th},i}^2$ describe, respectively, the shot noise and thermal noise in the ith pixel.

The shot-noise variance is given by [16]

$$\sigma_{\text{shot},i}^2 = 2erP_{b,i}\Delta f_n, \tag{22}$$

where e is the elementary charge, r is the photodiode responsivity (A/W), and Δf_n is the equivalent noise bandwidth of the preamplifier. Here, $P_{b,i}$ is the ambient light power incident on the ith pixel, which is given by [16]

$$P_{b,i} \approx 4\pi AB_{\text{sky}}\Delta\lambda T_F(\psi_i)T_L(\psi_i)\cos\psi_i \sin^2\left(\frac{\Psi_{a,i}}{2}\right), \tag{23}$$

where B_{sky} is the spectral radiance of the skylight (W/m^2·sr·nm), which is usually the dominant ambient light for an outdoor link and $\Delta\lambda$ is the bandwidth of the receiver optical filter. Here, ψ_i is the angle of the ray striking the center of the ith pixel with respect to the surface normal of the receiver, and $\Psi_{a,i}$ is the acceptance semi-angle of the ith pixel which is given by [24]

$$\Psi_{a,i} = 2\sin^{-1}\left(\frac{1}{\sqrt{N}}\sin\left(\frac{\text{FOV}}{2}\right)\right), \tag{24}$$

where the FOV of a receiver using a photodetector of total width w and a lens with a focal length f can be approximated by

$$\text{FOV} = 2\tan^{-1}\left(\frac{w}{2f}\right), \tag{25}$$

If the ambient light is uniform over the receiver FOV, to first order, the shot noise variance scales linearly with the pixel area and decreases as the number of pixels increases.

We assume that each pixel incorporates a transimpedance preamplifier. In general, thermal noise arises both from the feedback resistor and the transistors in the preamplifier, and has both white and non-white components. At sufficiently low bit rates (typically below 10 Mb/s), the white component is dominant [25], and contributes a variance

$$\sigma_{\text{th},i}^2 = \frac{4kT}{R_F}F_n\Delta f_n , \tag{26}$$

where k is Boltzmann's constant, T is the absolute temperature, R_F is the feedback resistance and F_n is the noise figure. As before, Δf_n is the equivalent noise bandwidth. The cutoff frequency (at -3 dB) is given by $B = G/2\pi R_F C_d$, where G is the open-loop voltage gain and C_d is the capacitance of a single pixel [16]. Assuming the detector has a fixed capacitance per unit area η , we have $C_d = \eta A_d$, where A_d is the area of a single pixel. We assume that the total power consumption of all N pixel preamplifiers is constrained. It can be shown that this is equivalent to constraining G. If the receiver is required to achieve a fixed cutoff frequency B, the feedback resistance must scale as $R_F = G/2\pi BC_d = G/2\pi B\eta A_d$, which is inversely proportional to the pixel capacitance or pixel area. The thermal noise variance becomes:

$$\sigma_{\text{th},i}^2 = \frac{8\pi kT}{G}\eta A_d F_n B\Delta f_n , \tag{27}$$

which is proportional to the pixel area, and thus inversely proportional to the number of pixels. Note that typically, both B and Δf_n scale in proportion to the bit rate.

Because the signal spot can overlap more than one pixel in an imaging receiver, the receiver can use different algorithms for detecting the signal. The simplest one is the select-best (SB) algorithm, where the receiver simply selects the pixel with maximum SNR and uses its output to detect the signal. In this algorithm, the outputs of all the other pixels are ignored. The SNR using SB is [16]

$$SNR_{\text{SB}} = \max_i\left(\frac{r^2 P_{\text{rec},i}^2}{\sigma_{\text{tot},i}^2}\right) = \max_i SNR_i \qquad 1 \leq i \leq N. \tag{28}$$

The SB algorithm is not optimal when the signal spot overlaps more than one pixel. In such cases, the optimal algorithm is maximal-ratio combining (MRC), where the receiver assigns different weights to different pixels and then sums the weighted outputs of all the pixels to form one signal, which is employed for signal decoding. The optimal weights for MRC are $\omega_i = rP_{\text{rec},i}/\sigma_{\text{tot},i}^2$ [16] and, therefore, the SNR using MRC is

$$SNR_{\text{MRC}} = \frac{\left(\sum_{i=1}^{N}\omega_i rP_{\text{rec},i}\right)^2}{\sum_{i=1}^{N}\omega_i^2\sigma_{\text{tot},i}^2} = \sum_{i=1}^{N}\frac{r^2 P_{\text{rec},i}^2}{\sigma_{\text{tot},i}^2} = \sum_{i=1}^{N}SNR_i . \tag{29}$$

This completes the analysis of an FSO link in the presence of atmospheric effects and misalignment between the transmitter and receiver. In the next section, we compare the two mechanisms by which atmospheric effects degrade the performance of FSO links: image blooming and attenuation of the received power.

3.2. Image blooming vs. attenuation

The first mechanism by which atmospheric effects degrade FSO link performance is signal attenuation, which arises both from absorption of light and from scattering of light out of the receiver FOV. We define the attenuation loss δ_{att} as the resulting decrease in receiver electrical SNR:

$$\delta_{\text{att}} = 20\log_{10}\left(\frac{P_{\text{fog}}}{P_{\text{air}}}\right) \qquad \text{(dB)}, \tag{30}$$

where P_{fog} and P_{air} are the total received optical powers in fog (or other atmospheric conditions) and clear air, respectively. As defined, δ_{att} does not depend on the operating SNR, the spatial distribution of noise, or the relative contributions of thermal noise and ambient-light shot noise.

The second mechanism by which atmospheric effects degrade FSO link performance is image blooming, which is the spreading of the signal spot over a larger number of pixels due to multiple scattering. We define the image blooming loss δ_{bloom} as the resulting decrease in receiver electrical SNR. Assuming the receiver employs MRC, this is given by

$$\begin{aligned}
\delta_{\text{bloom}} &= 10\log_{10}\left(\frac{SNR_{\text{MRC, fog}}}{SNR_{\text{MRC, air}}}\right) \\
&= 10\log_{10}\left(\frac{N_{\text{eff, air}}}{N_{\text{eff, fog}}}\right) \qquad \text{(dB)}.
\end{aligned} \tag{31}$$

In the first equality, $SNR_{\text{MRC, fog}}$ and $SNR_{\text{MRC, air}}$ are the SNR values in fog (or other atmospheric conditions) and clear air, respectively, computed using (29), assuming the noise is uniform across all pixels and is independent of weather conditions. The second equality defines $N_{\text{eff, fog}}$ and $N_{\text{eff, air}}$ as the effective number of pixels over which the image spot spreads in fog (or other atmospheric conditions) and clear air, respectively. Note that $N_{\text{eff, fog}}$ and $N_{\text{eff, air}}$ need not be integer-valued. Note also that, as defined, δ_{bloom} does not depend on the operating SNR or the relative contributions of thermal noise and ambient-light shot noise.

In order to compare the effects of image blooming and attenuation on FSO link performance, the SNR losses δ_{att} and δ_{bloom} for different weather conditions are shown in Fig. 5. The receiver uses a 28-mm *f*/2.8 lens and a photodiode having a total width of 19 mm. This corresponds to a horizontal FOV of 4 m at a distance of 6 m from the receiver, which is intended to be suitable for automotive applications. The transmitter comprises 12 LEDs uniformly spaced within a circle of 15-cm diameter, each emitting a first-order Lambertian pattern ($n = 1$ in (16)). The noise is assumed to be uniform across all pixels, and to be independent of atmospheric conditions. The forward scattering parameter and the visibility range are varied simultaneously based on values measured under different conditions [12, 21, 26], such that different parts of each plot correspond to different conditions (clear air, haze, fog and heavy rain). Fig. 5(a) considers a short link distance of 8 m, while Fig. 5(b) considers a longer link distance of 50 m. For both link distances, depending on the number of pixels, it is only at medium-to-heavy fog conditions that the attenuation loss exceeds the image blooming loss. Also, as expected, the image blooming loss increases with the number of pixels.
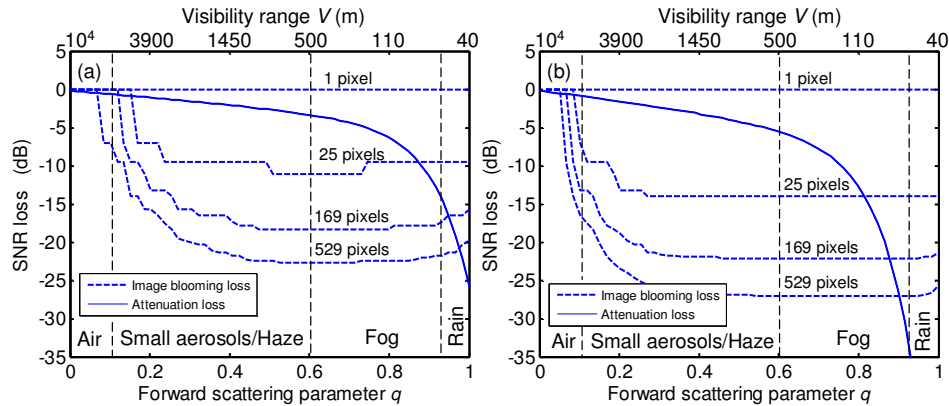
Fig. 5. SNR losses caused by image blooming and attenuation under different weather conditions (clear air to heavy rain) for receivers employing different numbers of pixels when the distance between the transmitter and receiver is (a) 8 m and (b) 50 m. Image blooming loss exceeds attenuation loss, except under medium-to-heavy fog conditions.

Fig. 6 shows the attenuation and image blooming losses versus link distance for a receiver with 169 pixels under three different weather conditions (haze, light fog and heavy fog). All other assumptions and parameters are the same as those in Fig. 5. Only at distances longer than 43 m and under heavy fog does the attenuation loss exceed the image blooming loss.

The results presented in this section demonstrate that the image blooming loss in imaging receivers can be significant, and should be included in any analysis of links in the presence of fog or other atmospheric effects. In the next section, we study the overall performance of FSO links in the presence of atmospheric effects.
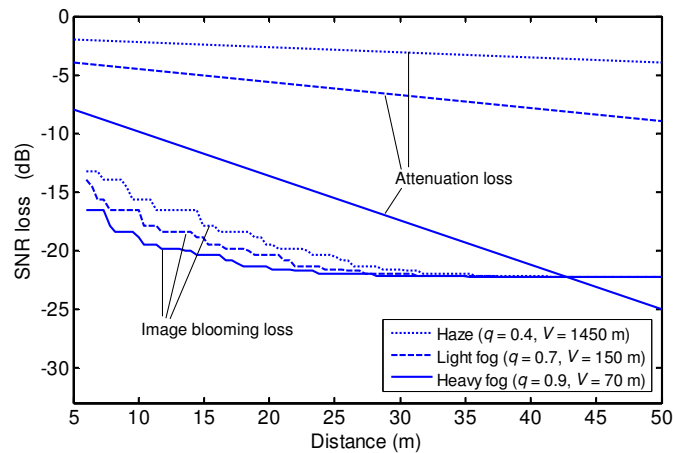

Fig. 6. SNR losses caused by image blooming and attenuation under three different weather conditions (haze, light fog and heavy fog) for an imaging receiver with 169 pixels, versus link distance. Image blooming loss exceeds attenuation loss except under heavy fog conditions at distances beyond 43 m.

3.3 Overall link performance

To demonstrate the overall effect of fog on the performance of FSO links employing imaging receivers, we have performed simulations varying the number of pixels, atmospheric conditions and link distance. The transmitter comprises 12 LEDs uniformly spaced within a circle of 15-cm diameter, each emitting a first-order Lambertian pattern ($n = 1$ in (16)), with a total power $P_{Tx} = 0.644 \, \text{W}$. The transmitter spectrum has 624-nm center wavelength and 18-nm FWHM. The bit rate is 100 kb/s, and the modulation is on-off keying with non-return-to-

zero pulse shape. The receiver uses a 28-mm f/2.8 lens, an optical bandpass filter with 624-nm center wavelength and 40-nm FWHM bandwidth, and a 19×19 mm^2 photodiode array having responsivity $r = 0.45$ A/W and capacitance per unit area $\eta = 0.6$ nF/cm^2. Each preamplifier has open-loop voltage gain $G = 10$, cutoff frequency $B = 100$ kHz, noise bandwidth $\Delta f_n = 140$ kHz and noise figure $F_n = 1.5$ dB. When present, ambient light is spatially uniform with spectral irradiance $B_{sky} = 0.13$ W/m^2·sr·nm, corresponding to a clear sky [27]. The shot and thermal noise variances $\sigma^2_{shot,i}$ and $\sigma^2_{th,i}$, computed using (22) and (27) respectively, both depend on the number of pixels. The transmitter is assumed to be pointed directly at the receiver ($\psi = \phi = 0$ in Fig. 4). To compute the average SNR for a set of system parameters, the transmitter is positioned at 100 different random locations within the receiver FOV on a plane parallel to the image plane. The receiver employs MRC.

Fig. 7 shows the average SNR versus link distance for receivers employing 1, 25 or 169 pixels in three different atmospheric conditions: clear air, light fog or heavy fog. The horizontal line indicates the minimum SNR required to achieve BER < 10^{-5}. Fig. 7(a) considers thermal noise only, and is relevant to transmission at night or to the common situation that the fog significantly attenuates the ambient light. Fig. 7(b) includes both thermal noise and shot noise from ambient light. It is fully realistic for reception in clear air, but is conservative for reception in heavy fog using a receiver with more than one pixel, because it is improbable (though not impossible) for a signal attenuated by fog to be spatially adjacent to a noise source not attenuated by fog. As expected, for each atmospheric condition and number of pixels, the link achieves a given SNR over longer distances in the absence of ambient light (Fig. 7(a)). Since the thermal and shot noise variances both scale linearly with the pixel area, for a given atmospheric condition, increasing the number of pixels leads to a higher SNR, whether ambient light is absent (Fig. 7(a)) or present (Fig. 7(b)). In both Figs. 7(a) and (b), the benefit of using more pixels is diminished as the atmospheric conditions worsen, and becomes minimal in the case of heavy fog. This is caused by image blooming, which spreads the signal spot over most of the photodetector area under heavy fog. In summary, Fig. 7 shows how fog can severely impair FSO link performance through the combined effects of image blooming and attenuation.
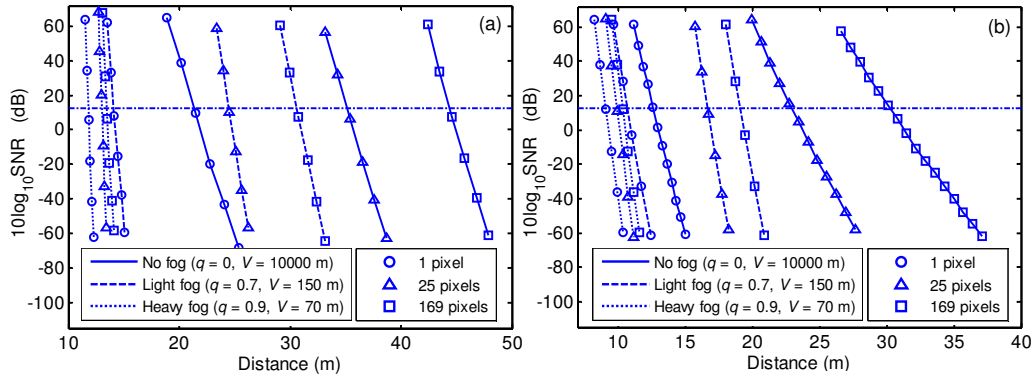

Fig. 7. Average SNR versus link distance in the presence of (a) thermal noise only or (b) thermal noise and ambient-light shot noise. The receiver employs 1, 25 or 169 pixels with MRC. Atmospheric conditions include no fog, light fog or heavy fog. For each curve shown, the SNR represents an average over 100 different transmitter locations within the receiver FOV. The horizontal line indicates the minimum SNR required to achieve a BER<10^{-5}.

4. Discussion

Solving the RTE for a generalized Lambertian source analytically is not an easily tractable problem, so our FSO link analysis was based on the APSF for an isotropic source. Transmitters in FSO links do not have isotropic radiation patterns, but many of them, such as those using LEDs designed for automotive applications, can be well modeled by first-order

Lambertian sources. When the misalignment between the transmitter and receiver is not very large, they behave similarly to an isotropic source. The model presented here is not expected to be valid when the transmitter is a highly directional source, such as a laser, and when there is a large misalignment between the transmitter and receiver. In such cases, accurate results can be obtained by either using a Monte-Carlo ray-tracing method [17], or by numerically solving the RTE for the specific source distribution considered.

5. Conclusion

In this paper we presented a theoretical framework for the analysis of FSO links using imaging receivers under different atmospheric conditions. The only parameters that one needs to know in order to be able to predict the effect of fog on link performance are the optical thickness T and the forward scattering parameter q of the atmosphere. We showed that atmospheric conditions degrade the performance of an FSO link by blooming the image of the signal spot and attenuating the received optical power. We compared these two effects under different atmospheric conditions and for different system parameters, and showed that except for cases of medium-to-heavy fog, image blooming loss is dominant over attenuation loss. We evaluated overall link performance under different atmospheric conditions. To the best of our knowledge, this is the first analysis of the effect of fog on FSO links with imaging receivers that takes image blooming into account.

Acknowledgments